文章编号：1001-9014(2022)03-0626-05

DOI:10.11972/j.issn.1001-9014.2022.03.014

Design of a novel Y-junction electro-optic modulator based on thin film lithium niobite

GUO Hong-Jie[1,3], LIU Hai-Feng[1*], WANG Zhen-Nuo[2,3], TAN Man-Qing[1,3*], LI Zhi-Yong[1], Lei Ming[4], GUO Wen-Tao[1]

(1. State Key Laboratory of Integrated Optoelectronics, Institute of Semiconductors, Chinese Academy of Sciences, Beijing 100083, China;
2. National Engineering Research Center for Optoelectronic Devices, Institute of Semiconductors, Chinese Academy of Sciences, Beijing 100083, China;
3. College of Materials Science and Opto-electronics Technology, University of Chinese Academy of Sciences, Beijing 100049, China;
4. State Key Laboratory of Inertial Technology, Beijing Institute of Automatic Control Equipment, Beijing 100074, China)

Abstract: In recent years, the high-performance electro-optic modulator based on the thin-film lithium niobate (TFLN) platform has been receiving considerable attention due to the featuring small footprint and low energy loss. In this paper, a novel Y-junction electro-optic modulator with a vertical electrode structure was designed based on TFLN. The relationship between the low half-wave voltage and the buffer layer thickness for the novel modulator was investigated. Meanwhile, the design parameters of Y-junction were optimized, and found that the half-wave voltage is less than 1.5 V and the insertion loss is less than 5 dB. Finally, the Y-junction electro-optic modulator was fabricated. This study not only provides insights on the design and realization of compact footprint photonic waveguides in the TFLN platform but also, experimental evidence for the fabrication of electro-optic modulators with high-performance and multifunction.

Key words: electro-optic modulator, TFLN, Y-junction waveguide

基于铌酸锂薄膜的Y波导集成调制器设计

郭宏杰[1,3], 刘海锋[1*], 王振诺[2,3], 谭满清[1,3*], 李智勇[1], 雷 明[4], 郭文涛[1]

(1. 中国科学院半导体研究所 集成光电子国家重点实验室, 北京 100083;
2. 中国科学院半导体研究所 光电子器件国家工程研究中心,北京 100083;
3. 中国科学院大学材料科学与光电工程中心, 北京 100049;
4. 北京自动控制设备研究所 国家重点惯性技术实验室,北京 100074)

摘要:近年来,基于薄膜铌酸锂(TFLN)平台的高性能电光调制器以其小体积、低能量损耗等特点受到广泛关注。本文提出了一种新的具有垂直电极结构的Y波导铌酸锂薄膜电光调制器。研究了调制器的半波电压与缓冲层厚度之间的关系,优化了Y波导的设计参数,最后设计得到插入损耗<5 dB, 半波电压<1.5 V的高性能调制器。本文不仅为基于TFLN平台的小型化波导的设计和实现提供了思路,而且为制造高性能和多功能的电光调制器提供了实验依据。

关 键 词:电光调制器;TFLN;Y波导

中图分类号:TN29　　**文献标识码**:A

Received date: 2021-08-16, **revised date**: 2022-02-28　　**收稿日期**:2021-08-16,**修回日期**:2022-02-28

Foundation items: Supported by Science and Technology Project of State Grid Corporation of China (No. 5700-202058482A-0-0-00), National Key Research and Development Program of China (No. 2019YFB2203802);

Biography: GUO Hong-Jie (1997-), male, Lishi, Ph. D student. Research area involves Electro-optic modulator and Electro-optic sensor. E-mail: guohongjie@semi.ac.cn.

* **Corresponding authors**: E-mail: liuhaifeng@semi.ac.cn, mqtan@semi.ac.cn

Introduction

In the last decades, photonic integrated circuits (PICs) have emerged as a mature and industrial platform, enabling the integration of active and passive optical components on a single chip in a scalable manner. Prominent PIC platforms, which are being developed to industrial scale, are silicon on insulator (SOI)[1, 2], silicon nitride (SiN)[3, 4], indium phosphate (InP)[5, 6], and lithium niobate (LN) [7, 8]. Lithium niobate ($LiNbO_3$, LN) is one of the most remarkable optical platforms due to its broad transparent windows and excellent electro-optic properties (γ_{33}= 31.2 pm/V). LN phase modulator (PM) is utilized as a tool to convert electrical signals into optical signals, and that plays vital roles in optical communication networks[9, 10], precision optical sensors[11, 12], quantum photonics[13], and non-reciprocal optics[14, 15].

Size and power efficiency are crucial to the application of the LN modulator. Conventional LN modulators are formed by low-index-contrast waveguides with weak optical confinement, which leads to the radius of bending and other adiabatic waveguides even up to 30 mm[16]. And the electrodes must be placed far away from the optical waveguide to minimize absorption losses, which leads to an increased drive voltage[17]. As a result, the conventional LN modulators are bulky in size and low in modulation efficiency (V_π *L*> *10 V cm*)[18, 19]. Recently, thin-film lithium niobate (TFLN) has emerged as a promising platform for excellent and compact electro-optic modulator, which unlocks new levels of performance and footprint in LN modulators because it overcomes the fundamental voltage-size trade-off in conventional low-index-contrast LN modulators[20, 21].

In this paper, a novel Y-junction electro-optic PM based on the TFLN platform was analyzed, simulated, and designed. The low half-wave voltage versus the thickness of the buffer layer was analyzed. The propagation losses of LN waveguides with different separation distances were optimized using the Beam Propagation Method (BPM). Finally, the designed electro-optic modulator features low optical loss (<5 dB), low V_π(<1.5 V), and a small footprint(<2 cm), compared with the conventional LN counterpart. The results obtained in this paper can provide useful insight into the design of high-performance and multifunction electro-optic modulators.

1　Design and materials

The device studied in this paper was a Z-cut TFLN deposited on an LN substrate, which utilizes the maximum electro-optic coefficient γ_{33}. Fig. 1(a) shows the schematic diagram of the TFLN electro-optic PM. In Fig. 1(a), The polarizer (L_1) is realized with a metallic overlay that absorbs the TM mode, which could provide high polarization rejection based on a proton exchange waveguide. The Y-junction (L_2) is a 3 dB passive waveguide coupler, which is the optimal technological compromise for high-performance fiber optical gyroscopes (FOG). Metallic electrodes are fabricated vertically above the waveguide to achieve phase modulation (L_3). The end-face coupling technique is employed to couple the LN substrate with the fiber. Fig. 1(b) shows the cross-section of the TFLN modulator. The vertical electrode configuration based on the TFLN slab not only reduces the electrode gap but also increases the integral Γ as shown in Fig. 1(b). To avoid optical absorption resulting from the electrodes placed directly above the waveguide, a buffer layer of SiO_2 thin film was inserted between the TFLN slab and the electrodes.

2　Analyze and simulation

When the light wave travels through a modulation length of L, the phase change can be expressed as:

$$\Delta\varphi = \Delta\beta \cdot L = \frac{2\Delta n_e \pi L}{\lambda} = n_e^3 \gamma_{33} \frac{\pi L \Gamma}{\lambda} E \quad , \quad (1)$$

where $\Delta\beta$ is the change of propagation constant induced by the applied electric field, n_e is the refractive index of the extraordinary lightwave, Δn_e is the change of refractive index induced by the applied electric field, γ_{33} is the electro-optic coefficient of lithium niobite crystal, E is applied electric field in the waveguide, and Γ is the electro-optic integral factor between the electric field and optical field.

For the traditional bulk LN PM, the applied voltage corresponding to a phase change of π, generally known as half-wave voltage, can be expressed as:

$$V_\pi = \frac{\lambda G}{2 n_e^3 \gamma_{33} L \Gamma} \quad . \quad (2)$$

According to Eq. (2), it is found that the proper method of decreasing V_π for a fixed modulation length L is to narrow the electrode gap G or improve the electro-optic integral factor Γ. Generally, the electrode gap should be maintained at a certain distance so as to avoid possible optical absorption of the waveguide. The integral Γ cannot be increased dramatically for the coplanar electrode structure on the surface of the LN crystal. Therefore, the

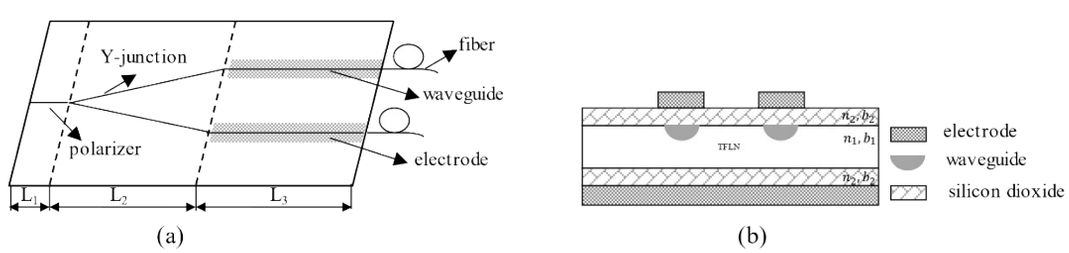

Fig. 1　(a) The schematic diagram of the TFLN PM, (b) the cross section of the TFLN PM
图 1　(a) TFLN 相位调制器结构示意图, (b) TFLN 相位调制器波导截面结构

above methods are inappropriate for the traditional LN fabricated on bulk LN PM. The TFLN PM with a vertical electrode is beneficial for shortening the G and increasing the integral Γ simultaneously. Compared to the integral Γ of 40%~50% for the electrode configuration in bulk LN crystal, Γ can be as high as 90~100% for the vertical electrode structure. In Fig. 1(b), the buffer layer thickness is b_2 and the corresponding refractive index (n_2) is 1.45. The thickness of TFLN slab is b_1 and the refractive index (n_1) is 2.21. According to the boundary conditions of the electromagnetic fields (see Eq. (3) and Eq. (4)), the V_π of TFLN PM can be expressed as:

$$n_1^{1/2}E_1 = n_2^{1/2}E_2 \quad , \quad (3)$$

$$V = E_1 b_1 + 2E_2 b_2 \quad , \quad (4)$$

$$V_\pi = \frac{\lambda}{2n_1^3\gamma_{33}L\Gamma}\left(b_1 + 2b_2\sqrt{\frac{n_1}{n_2}}\right) \quad . \quad (5)$$

Fig. 2 (a) shows the V_π of conditional bulk PM as a function of G at the modulation length L of 5 mm, 10 mm, 20 mm, and the integral Γ of 50%. Fig. 2 (b) shows the V_π of TFLN PM as a function of b_2, with Γ= *90%* and b_1=*5 μm*. Compared with bulk LN PM, the V_π of TFLN PM can be dramatically decreased when the same modulation length is adopted. This is beneficial for the high-performance PIC. Moreover, it is also observed that when *L>10 mm*, the V_π would be less than 1.5 V. So, to meet the circuit design, the L_3=*1000 μm* is taken into account in our proposed modulator.

Fig. 3(a) shows the schematic diagram of the Y-junction composed of two identical S-waveguides. The distance between the S-waveguide, width, height, length, and bending angle of the S-waveguide are denoted as W, w, h, L_2, and α, respectively. Fig. 3(b) shows the W as a function of L_2 under the different bending angle α. From Fig. 3(b), it is found the W increases with the increase of the modulation length L_2. Besides, the W decreases as the bending angle α decreases. In order to cut down the footprint of the modulator and reduce the propagation loss of light, it is also necessary to optimize the parameters of Y-junction waveguide. In addition, W should satisfy the empirical value *150 μm* ≤W≤*400 μm*, which matches the V-groove coupling process[22]. So, the light-guiding properties of the Y-junction waveguide (h=*7 μm*, w=*7 μm*, Δn=*0.015*, α=*0.4~1.0°* and L_2=*0.4~1.2 cm*) are simulated using the BPM method with RSoft commercial software.

Fig. 4(a) shows the normalized input power to the output ports as the input field propagates through the Y-junction. From Fig. 4(a) it can be seen that the output

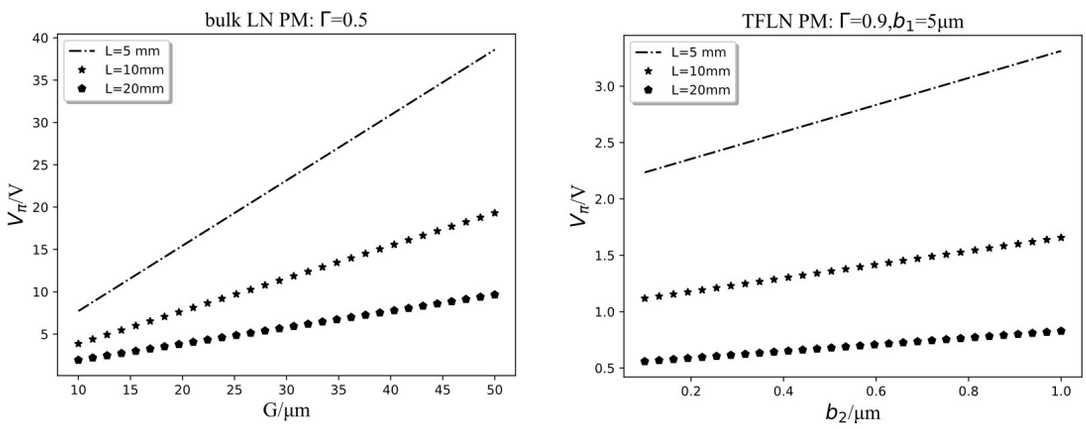

(a) (b)

Fig. 2 (a) The V_π of conditional bulk PM various G at different modulation length, where Γ = 0.5, (b) the V_π of TFLN PM various b_2 at different modulation length, where Γ = 0.9, b_1=*5 μm*

图2 (a) 不同调制长度下,传统体相位调制器G与半波电压Vπ关系图,其中Γ = 0.5,(b) 不同调制长度下,薄膜相位调制器b2与半波电压Vπ关系图,其中Γ = 0.9,b1=5 μm

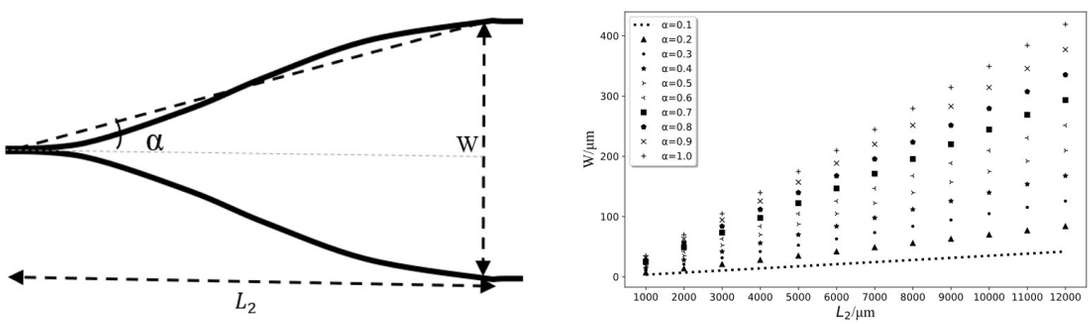

(a) (b)

Fig. 3 (a) The sketch of Y-junction waveguide, (b) the W of Y-junction waveguide versus L_2 at different α

图3 (a) Y波导结构,(b) 在不同α下,Y波导W与L2的关系图

power decreases with the increase of the L_2. Besides, the output power also decreases as the bending angle α increases. In order to balance the loss and the manufacturing process, $\alpha=0.6^\circ$ and $L_2=9000\ \mu m$ are selected as the optimal parameters. The simulation results of $\alpha=0.6^\circ$ and $L_2=9000\ \mu m$ are shown in Fig. 4(b-c). The simulated result (Fig. 4(b)) shows the refractive index profile of waveguide section when $L_2=100\ \mu m$. Fig. 4(c) shows the electric field distribution inside the Y-junction waveguide. It is obvious that there exists and clearly shows an almost equal splitting of input power into two branches.

The overall insertion loss (coupling loss and propagation loss) of the TFLN PM with the 7 μm diameter fiber is simulated using the BPM method by RSoft. The simulation result is shown in Fig. 5. It is can be seen that the overall insertion loss is 4.7 dB. Meanwhile, it is also observed that the coupling loss almost accounts for 94% of the insertion loss, which is caused by the mismatch of the optical mode field. The mode field mismatch loss can be expressed by the following formula Eq. (6)

$$POI = \frac{\left|\iint \phi_f(x,y)\phi_w^*(x,y)dxdy\right|^2}{\iint\left|\phi_f(x,y)\right|^2 dxdy * \iint\left|\phi_w(x,y)\right|^2 dxdy}, \quad (6)$$

where $\phi_f(x,y)$ is the mode field distribution of fiber, $\phi_w(x,y)$ is the mode field distribution of waveguide. This paper simulates the result of a direct connection between the flat-end optical fiber and the untreated waveguide end face. Due to the weak ability of the diffused waveguide to restrict the optical field, the diameter of waveguide mode field distribution $\phi_w(x,y)$ (about 10 μm) is larger than that of fiber field distribution $\phi_f(x,y)$ (6 μm), which leads to a mode field mismatch. The $\phi_w(x,y)$ can be reduced by adding a spot-size converter(SSC) to the output of the waveguide, and then a lower coupling loss is obtained.

3 Experimental verification

Fig. 6 shows the cross-section of the TFLN slab bonded on the LN substrate. The anneal proton exchange waveguide (w=7 μm, h=7 μm, L_1=1 000 μm, L_2=9 000 μm, L_3=10 000 μm) was fabricated on the Z-cut thin-film lithium niobite slab on a bulk LN substrate. The bright stripe in the middle is the TFLN slab and the slightly darker area underneath is the bulk LN substrate.

The Z-cut thin-film lithium niobite wafer on bulk LN substrate was fabricated by the direct bonding technology and chemical mechanical polishing process, and a thin film of $10\ \mu m$ was obtained. Subsequently, the proton exchange process was performed by immersing the TFLN wafer into the benzoic acid melt with lithium benzoate, which started at a temperature of around 200 ℃ and lasted for about 4~5 hours. And afterward, the TFLN chip was placed at the center of a three-zone diffusion furnace. The thermal annealing process was performed at a temperature of around 330 ℃. The wafer was placed at the furnace lasting for several hours. Finally, the TFLN waveguide wafer was diced into individual chips and the endfaces were polished.

The insertion loss of the TFLN waveguide was characterized based on the butt-coupling method at the wavelength of 1310 nm. A polarization-maintaining fiber with a mode field diameter (MFD) of $6.0\pm0.5\ \mu m$ was placed at the input port and output port of the TFLN waveguide sample. An insertion loss of $\sim5.0\ dB$ was obtained using an SLD light source, and it is limited by the waveguide coupling method of the V-groove process. This value could be further increased by the edge coupling method[23].

4 Conclusion

In conclusion, a novel Y-junction electro-optic PM was analyzed, simulated, and designed. The correlation of the low half-wave voltage and thickness of the buffer

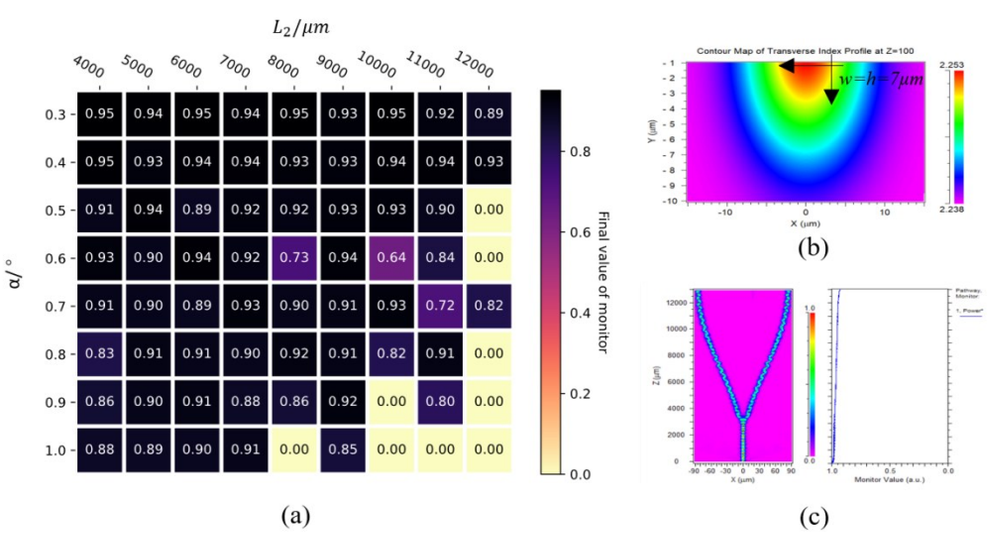

Fig. 4 (a) The results of BPM simulation, (b) the refractive index profile of waveguide section, (c) the power distribution of Y-junction waveguide

图4 (a) BPM 仿真结果图, (b) 波导截面折射率分布图, (c) Y 波导能量分布仿真图

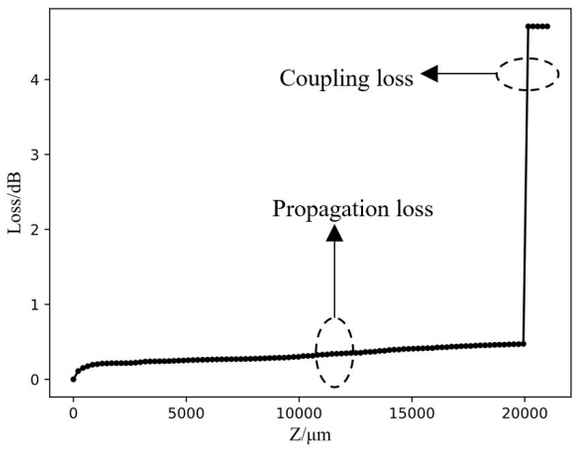

Fig. 5 The results of simulation modulator insertion loss, where L_1=1 000 μm, L_2=9 000 μm, L_3=10 000 μm, α=0.6°
图5 模拟调制器插入损耗的结果,其中L1=1 000 μm,L2=9 000 μm,L3=1 0000 μm, α=0.6°

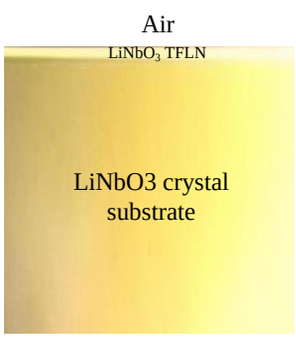

Fig. 6 The microscope image of the cross-section of the TFLN slab bonded on the LN substrate
图6 基于LN衬底的TFLN调制器显微镜成像图

layer was analyzed. It is found there exists a negative correlation between the low half-wave voltage and thickness of the buffer layer. The V_π of TFLN PM can be dramatically decreased when the same modulation length is adopted compared with that of the bulk LN PM, which is beneficial for the high-performance PIC. Moreover, the propagation losses of LN waveguides with different separation distances of the waveguide were optimized by the BPM method. It is found that the overall insertion loss is 4.7 dB. Finally, an on-chip PM with low optical loss (< 5 dB) and a smaller footprint(<2 cm) was fabricated.

References

[1] Leuthold J, Koos C, Freude W. Nonlinear silicon photonics [J]. *Nature Photonics*, 2010, **4**(8): 535-544.
[2] Lim A E J, Song J F, Fang Q, *et al*. Review of Silicon Photonics Foundry Efforts [J]. *IEEE Journal of Selected Topics in Quantum Electronics*, 2014, **20**(4).
[3] Roeloffzen C G H, Zhuang L M, Taddei C, *et al*. Silicon nitride microwave photonic circuits [J]. *Optics Express*, 2013, **21**(19): 22937-22961.
[4] Gao Y, Zhou G D, Zhao N, *et al*. High-performance chemical vapor deposited graphene-on-silicon nitride waveguide photodetectors [J]. *Optics Letters*, 2018, **43**(6): 1399-1402.
[5] Nagarajan R, Kato M, Lambert D, *et al*. Terabit/s class InP photonic integrated circuits [J]. *Semiconductor Science and Technology*, 2012, **27**(9).
[6] Nagarajan R, Kato M, Pleumeekers J, *et al*. InP Photonic Integrated Circuits [J]. *IEEE Journal of Selected Topics in Quantum Electronics*, 2010, **16**(5): 1113-1125.
[7] Tran M A, Komljenovic T, Hulme J C, *et al*. Integrated optical driver for interferometric optical gyroscopes [J]. *Optics Express*, 2017, **25**(4): 3826-3840.
[8] Bai B, Bai Y, Li D, *et al*. Double Q-switched 946 nm laser with MgO: LN electro-optic crystal and MoSe2 saturable absorber [J]. *Chinese Optics Letters*, 2018, **16**(3).
[9] Kovalevich T, Belharet D, Robert L, *et al*. Bloch surface waves at the telecommunication wavelength with lithium niobate as the top layer for integrated optics [J]. *Applied Optics*, 2019, **58**(7): 1757-1762.
[10] Chang Z S, Jin W, Chiang K S. Graphene electrodes for lithium-niobate electro-optic devices [J]. *Optics Letters*, 2018, **43**(8): 1718-1721.
[11] Chamoun J, Digonnet M J F. Aircraft-navigation-grade laser-driven FOG with Gaussian-noise phase modulation [J]. *Optics Letters*, 2017, **42**(8): 1600-1603.
[12] Nikitenko A N, Volkovskiy S A, Mikheev M V, *et al*. Influence of Acousto-Optic Resonances in Electro-Optical Modulator on Fiber Optic Gyro Performance and Method for Its Compensation [J]. *IEEE Sensors Journal*, 2018, **18**(1): 273-280.
[13] Krasnokutska I, Tambasco J L J, Li X J, *et al*. Ultra-low loss photonic circuits in lithium niobate on insulator [J]. *Optics Express*, 2018, **26**(2): 887-894.
[14] Luo R, Jiang H W, Rogers S, *et al*. On-chip second-harmonic generation and broadband parametric down-conversion in a lithium niobate microresonator [J]. *Optics Express*, 2017, **25**(20): 24531-24539.
[15] Xue W, Qiao-Fen Z, Yan Z. Generation of arbitrary terahertz pulse in non periodically poled lithium niobate [J]. J. Infrared Millim. Waves, 2010, **30**(3): 221~223.(毋雪, 朱巧芬, 张岩.基于非周期极化铌酸锂晶体产生任意频率太赫兹辐射.**红外与毫米波学报**), 2010,**30**(3): 221~223.
[16] Deppe O, Dorner G, König S, *et al*. MEMS and FOG Technologies for Tactical and Navigation Grade Inertial Sensors—Recent Improvements and Comparison [J]. 2017, **17**(3): 567.
[17] Slavik R, Farwell S G, Wale M J, *et al*. Compact Optical Comb Generator Using InP Tunable Laser and Push-Pull Modulator [J]. *IEEE Photonics Technology Letters*, 2015, **27**(2): 217-220.
[18] iXBlue. lithium niobate electro-optic modulator products, [OL], (2021)[*2021*], https://photonics.ixblue.com/store/lithium-niobate-electro-optic-modulator/phase-modulators.
[19] Optical. lithium niobate electro-optic modulator products, [OL], (2021)[*2021*], https://www.optilab.com/optical-modulator.
[20] Boes A, Corcoran B, Chang L, *et al*. Status and Potential of Lithium Niobate on Insulator (LNOI) for Photonic Integrated Circuits [J]. *Laser & Photonics Reviews*, 2018, **12**(4).
[21] Krasnokutska I, Tambasco J-L J, Li X, *et al*. Ultra-low loss photonic circuits in lithium niobate on insulator [J]. *Optics Express*, 2018, **26**(2): 897-904.
[22] Zijun T, Wenfeng C, Hao W, *et al*. Research on Direct Couping of PM Fiber Coil and Y-branch LiNbO3 Waveguide Chip [J]. Semiconductor Optoelectronics, 2017, **38**(01): 57-60.(田自君, 蔡文峰, 吴昊, 等.保偏光纤环与Y波导芯片直接耦合技术研究.**半导体光电**), 2017,**38**(01): 57-60.
[23] Ying P, Tan H Y, Zhang J W, *et al*. Low-loss edge-coupling thin-film lithium niobate modulator with an efficient phase shifter [J]. *Optics Letters*, 2021, **46**(6): 1478-1481.